Enhanced adsorption of methylene blue onto graphene oxide-doped XFe_2O_4 (X = Co, Mn, Ni) nanocomposites: kinetic, isothermal, thermodynamic and recyclability studies

Long Giang Bach, Thuan Van Tran, Trinh Duy Nguyen, Thinh Van Pham & Sy Trung Do

Research on Chemical Intermediates

ISSN 0922-6168

Res Chem Intermed
DOI 10.1007/s11164-017-3191-1

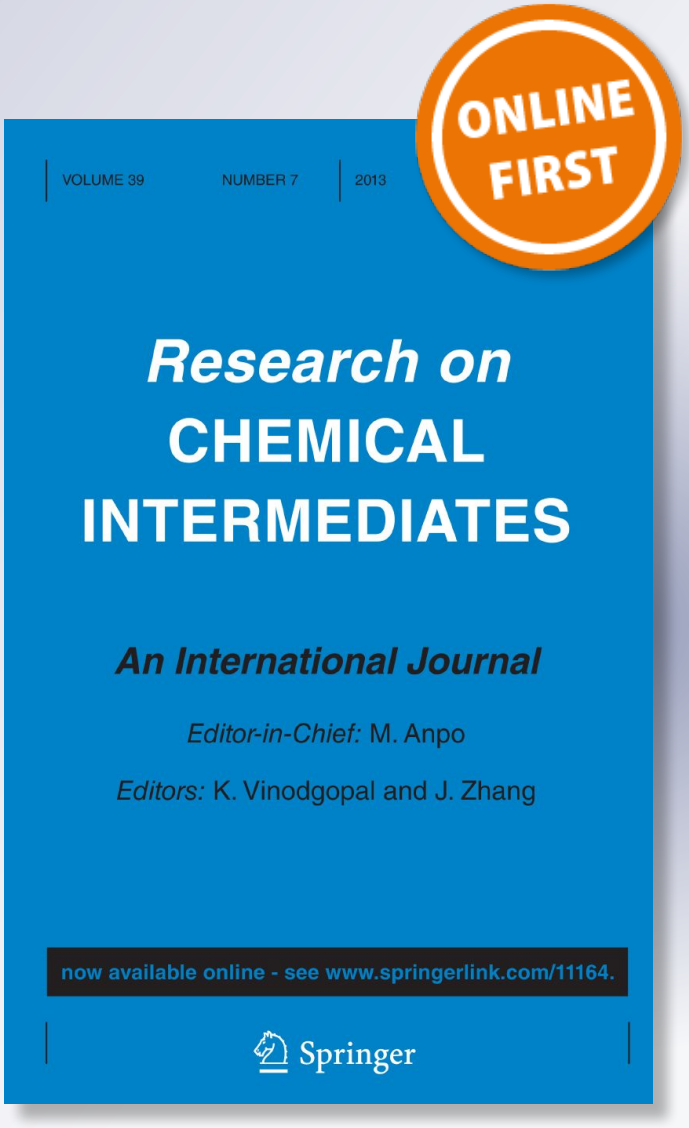

Springer

Res Chem Intermed
https://doi.org/10.1007/s11164-017-3191-1

Enhanced adsorption of methylene blue onto graphene oxide-doped XFe_2O_4 (X = Co, Mn, Ni) nanocomposites: kinetic, isothermal, thermodynamic and recyclability studies

Long Giang Bach[1] · Thuan Van Tran[1] · Trinh Duy Nguyen[1] · Thinh Van Pham[2,3] · Sy Trung Do[4]

Received: 25 July 2017 / Accepted: 30 October 2017

Abstract The nanocomposites XFe_2O_4/GO with various metal sites (X = Co, Mn, and Ni) were successfully synthesized via the polymerized complex method. The XFe_2O_4/GO family was characterized using X-Ray diffraction analysis, scanning electron microscopy (SEM), and a vibrating sample magnetometer. We also investigated the effect of three fundamental parameters (initial concentration, dosage, and pH) on the removal of methylene blue using the response surface methodology. A high F value, very low P value (< 0.00001), a non-significant lack of fit, and the determination coefficient ($R^2 > 0.95$) demonstrated a strong correlation between experimental and predicted values of the responses. The predicted optimal conditions for maximum removal efficiency were easily determined to adhere to the following trend for actual test experiments: $MnFe_2O_4$/GO (60.1%) < $CoFe_2O_4$/GO (80.3%) < $NiFe_2O_4$/GO (87.7%). Moreover, the adsorption behavior was well-described by the Langmuir isotherm and a pseudo-second-order kinetic model. The maximum capacity for adsorption of methylene blue onto XFe_2O_4/GO was found from 42.2 to 80.6 mg/g. Moreover, the XFe_2O_4/GO could be regenerated for several cycles without a considerable decrease in removal yield, suggesting that this highly promising XFe_2O_4/GO could be applied as an efficient and novel adsorbent.

✉ Long Giang Bach
blgiang@ntt.edu.vn

[1] NTT Institute of High Technology, Nguyen Tat Thanh University, Ho Chi Minh City, Vietnam

[2] Graduate University of Science and Technology, Vietnam Academy of Science and Technology, Ho Chi Minh City, Vietnam

[3] Dong Nai Technology University, Bien Hoa, Dong Nai Province, Vietnam

[4] Laboratory of Material and Environment Technology, Institute of Chemistry, Vietnam Academy of Science and Technology, Hanoi City, Vietnam

Published online: 05 December 2017

Keywords Magnetic nanoparticle · Graphene oxide · Response surface methodology · Adsorption kinetic and isotherms · Desorption and recyclability

Introduction

Synthetic dyes and pigments are organic compounds with chemical structures consisting of two major components: chromophores, which are responsible for producing the colors, and auxochromes, which enhance water solubility [1]. They have recently played a fundamental role in the manufacture of textiles, paper, plastic, and pharmaceuticals due to their advantageous characteristics, including high solubility in polar solvents, straightforward synthetic access, and excellent compatibility with fabrics [2].

Methylene blue (MB; 3,7-bis(dimethylamino)phenothiazin-5-ium chloride) is a cationic organic dye. Despite the use of MB in low concentrations, it is a non-biodegradable substrate, and its presence in excess quantities poses a threat to human health and the environment. Conventional approaches for the treatment of MB-containing industrial effluents, such as Fenton oxidation, irradiation, photocatalytic degradation, and membrane filtration, have garnered the attention of scientists worldwide. Among the routes mentioned, elimination of dyes from wastewater via the adsorption technique is especially promising, as this method is characterized by remarkable effectiveness and good recyclability; hence, low-cost porous adsorbents have become increasingly popular.

Graphene nanomaterial is composed of two-dimensional sp^2-hybridized carbon single layers, where atoms are arranged in a hexagonal crystal structure [3]. Graphene-based materials such as graphene oxide (GO), which is exfoliated by chemical oxidation, exhibit several properties essential for the capture of dye molecules, including a surface marked by diverse nitrogen- and oxygen-containing functional groups and a large surface area with a wide range of highly porous sites. However, it is difficult to separate dye-adsorbed GO from water because this nanomaterial is characterized by relatively low density d (GO/H_2O) = 1.26. The separation of dye-adsorbed GO after adsorption by combining the nanomaterials with strong magnetic components to form the XFe_2O_4 graphene oxide nanocomposites (XFe_2O_4/GO) represents a feasible novel strategy. Therefore, this material might be amenable to magnetic separation and recycling.

Herein, we describe the preparation of XFe_2O_4/GO nanocomposites via a simple polymerized complex route. The properties of the synthesized XFe_2O_4/GO were characterized using several physical techniques, including scanning electron microscopy (SEM), X-ray powder diffraction (XRD), and measurement using a vibrating-sample magnetometer (VSM). The XFe_2O_4/GO was used as an adsorbent to eliminate MB from aqueous solution. In addition, a series of input factors affecting the adsorption process designed using response surface methodology (RSM) were investigated [4, 5], and adsorption behavior was also explored through the adsorption models. Finally, desorption and recyclability were also studied.

Experimental procedure

Chemicals and instruments

All chemicals for this study were commercially purchased from Merck and used as received without further purification unless otherwise noted. All samples were pretreated by heating at 105 °C for 1 h. The XRD of XFe_2O_4/GO composites was carried out on a Bruker D8 Advance powder diffractometer with a Cu–Kα excitation source and a scan rate of 0.02°/s from 10° to 90°. SEM was recorded on a Hitachi S-4800 instrument (Japan), using an accelerating voltage source of 10 kV with magnification of $\times$7000. The magnetic properties were studied using a VSM. Absorption spectra were obtained using a UV–Vis spectrophotometer.

Preparation of GO

GO was synthesized from natural graphite powder exfoliated using common oxidants [6]. First, graphite (3.0 g) was combined with 150 mL of concentrated H_2SO_4 (98%) in a 500-mL flask and stirred in an ice bath (3–5 °C). Then, 10.5 g $KMnO_4$ was slowly added to the solution over the course of 20 min, and the resulting mixture was stirred for an additional 20 min at the same temperature. After the solution was warmed to room temperature amd stirred for 24 h, 250 mL of deionized water was slowly added to mixture with stirring, followed by the slow addition of 5 mL H_2O_2 (30 wt%) until a golden yellow solution was obtained. Finally, the products were filtered and washed three times with HCl (1 L, 3%), followed by deionized water (1 L). The GO product was suspended in distilled water and dialyzed with deionized water overnight to remove metal ions and acids. The resulting GO solution was diluted with water to a concentration of 3 g/L. The concentration of GO in solution is estimated by the initial carbon source used to prepare GO based on the assumption that no carbon is lost during the synthesis of the final product.

Preparation of XFe_2O_4 by polymerized method

Transition metal-based magnetic nanoparticles were prepared by a polymerized complex method [7]. First, citric acid (93 g), ethylene glycol (40 mL), and deionized water (100 mL) were dissolved completely at 80 °C. Then, the chloride $XCl_2{\cdot}6H_2O$ (0.36 g $CoCl_2{\cdot}6H_2O$; 0.303 g $MnCl_2{\cdot}6H_2O$; 0.36 g $NiCl_2{\cdot}6H_2O$) and 0.5 g $FeCl_3{\cdot}6H_2O$ were added. The mixtures were stirred at 130 °C to obtain the polymeric resin. The precursor was then heated in an open-air furnace at 1000 °C for 2 h.

Preparation of XFe_2O_4/GO nanocomposites

The XFe_2O_4/GO composites were synthesized as reported previously [8]. In a typical experiment, a beaker containing 50 mL ethanol and 1.0 g XFe_2O_4, and a second beaker containing 5 mL GO colloidal suspension and 45 mL water were

both subjected to ultrasonication for 1 h. The contents of the two beakers were then transferred to a 500-mL beaker, and the resulting mixture was stirred at 60 °C to vaporize. The solid was dried continuously at 90 °C and subsequently used for the experimental runs.

Experimental batch

Batch tests in this study were carried out at room temperature, and adsorption was allowed to proceed for 3 h. The adsorption experiments were carried out in an Erlenmeyer flask containing 100 mL of an aqueous solution of MB. After the adsorption equilibrium was obtained, the XFe_2O_4/GO adsorbents were removed from the mixture using magnetic and centrifugal methods. The residual concentrations were confirmed by UV–Vis spectroscopy, and MB removal was calculated by the following equation:

$$\text{MB removal } (\%) = \frac{C_o - C_e}{C_o} \cdot 100 \tag{1}$$

where C_o and C_e are initial and equilibrium MB concentrations (ppm), respectively.

The adsorption capacity was calculated as follows:

$$q_e(\text{mg/g}) = \frac{C_o - C_e}{W} \cdot V \tag{2}$$

where V (mL) is the volume of the MB solution, and W (g) is the weight of XFe_2O_4/GO.

Determination of pH point of zero charges (pHzpc)

The pHzpc is a crucial parameter for evaluating acidity/basicity and net surface charge of any adsorbent in a solution. The procedure for pHzpc determination was the same as that described in our previous [9]. In a typical experiment, XFe_2O_4/GO ($m_o = 0.05$ g) was added to flasks containing 50 mL of KCl (0.1 mol/L) at different pH values ($pH_o = 2, 4, 6, 8, 10, 12$). The solutions were kept stable over the course of 24 h, and the solids were removed from the mixture. The final pH was then measured using a pH meter. A curve of the final pH against the initial pH was plotted, and the pHpzc was calculated at pH initial = pH final.

Experimental design with RSM

The RSM technique is applied to assess experimental results through second-order polynomial regression equations which describe the mathematical relationship between the response (y) and the set of independent values (x) as the following equation:

$$\beta_o + \sum_{i=1}^{k} \beta_i x_i + \sum_{i=1}^{k} \sum_{j=1}^{k} \beta_{ij} x_i x_j + \sum_{i=1}^{k} \beta_{ii} x_i^2 \quad (3)$$

where y is the predicted response, and x_i and x_j are the independent variables (i, $j = 1, 2, 3, 4 \ldots k$). The parameter β_o is the model constant, β_i is the linear coefficient, β_{ii} is the second-order coefficient, and β_{ij} is the interaction coefficient. Central composite design (CCD) is used to design the given experiments. Analysis of variance (ANOVA) is performed using the Design-Expert version 9.0.5.1 (DX9) software program, which provides an efficient means of data analysis (Table 1).

Results and discussion

Textural characterization of XFe_2O_4/GO

The crystalline structure of various XFe_2O_4/GO adsorbents was first investigated using XRD, and a diagram of the spectrum is shown in Fig. 1a. The characteristic peak of GO at low-angle $2\theta = 10.4°$ was absent from the given diagram at the respective positions, suggesting that the graphene oxide was highly reduced via bond formation with XFe_2O_4 [10]. Moreover, other significant diffraction peaks for $CoFe_2O_4$/GO (30.3°, 34.2°, 44.3°, 57.1°), $MnFe_2O_4$/GO (26.2°, 42.9°, 54.4°, 64.4°), and $CoFe_2O_4$/GO (26.4°, 30.4°, 35.8°, 43.4°, 63.0°) revealed that the crystalline nature fit well with the spinel structure of ferrites reported in previous studies [11–13].

The magnetization curves of XFe_2O_4/GO obtained via the VSM technique are plotted in Fig. 1b. The saturation magnetization values were found to follow the order: $MnFe_2O_4$/GO (1.57 emu/g) < $NiFe_2O_4$/GO (2.38 emu/g) < $CoFe_2O_4$/GO (4.49 emu/g). This arrangement is also in accord with the recorded magnetization of ferrite XFe_2O_4, although the measured magnetization values of XFe_2O_4/GO in the present study are lower than those of the respective ferrites [14]. Decreased magnetization can be attributed to the presence of non-magnetic graphene covering the surface of these ferrites [15]. However, the magnetization obtained is advantageous for the separation of XFe_2O_4/GO from aqueous solution by inducing an external magnetic field. The pHpzc of $CoFe_2O_4$/GO, $MnFe_2O_4$/GO, and $NiFe_2O_4$/GO were found to be 6.4, 7.2, and 7.1, respectively (Fig. 1c). The SEM

Table 1 Independent variables matrix and their encoded levels for XFe_2O_4/GO (X = Co, Mn, Ni)

No.	Independent factors	Code	Levels				
			− α	− 1	0	+ 1	+ α
1	Initial concentration (mg/L)	x_1	66.4	80	100	120	133.6
2	Adsorbent dosage (g/L)	x_2	0.16	0.5	1	1.5	1.84
3	pH of solution (–)	x_3	3.6	5	7	9	10.4

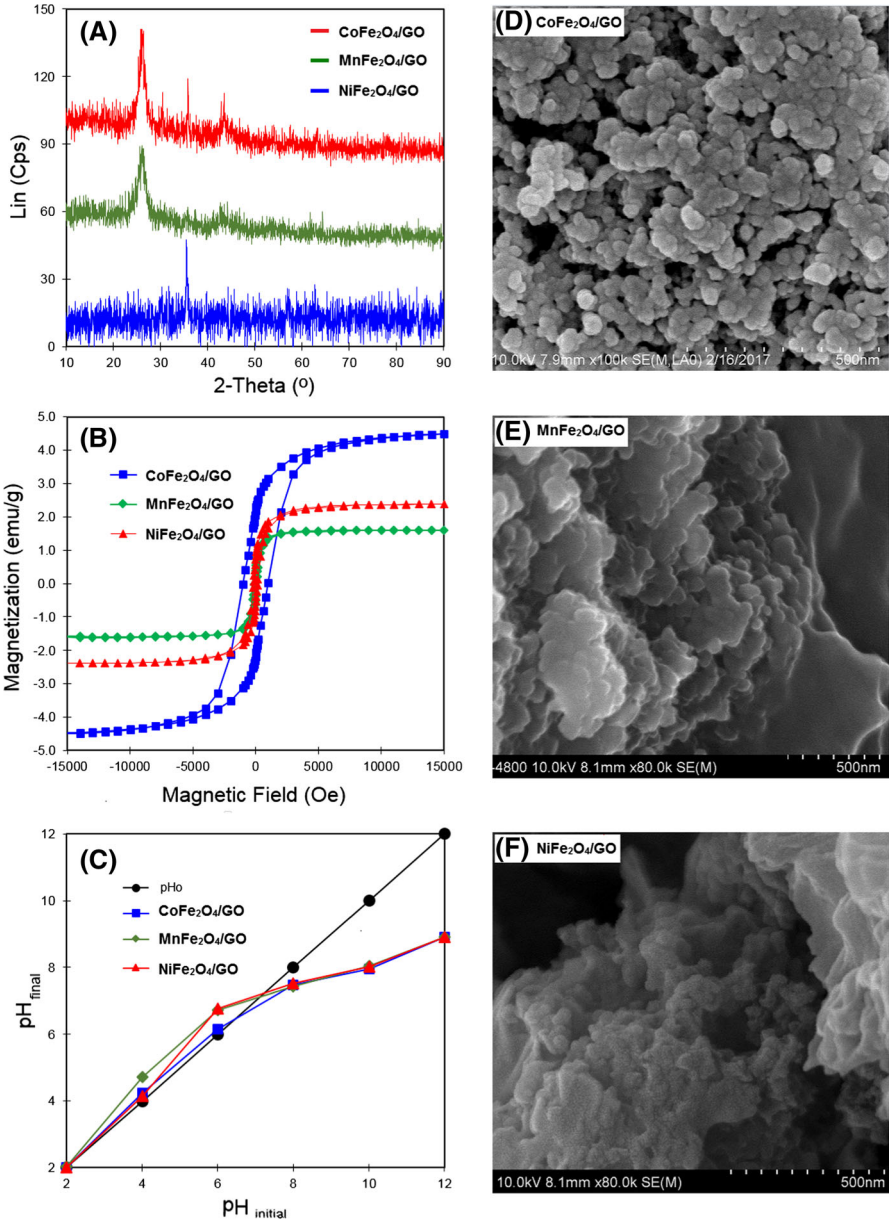

Fig. 1 XRD spectra (**a**), VSM (**b**), pHpzc (**c**), and SEM images (**d–f**) of XFe_2O_4/GO (X = Co, Mn, Ni)

spectra profile in Fig. 1d–f compares the difference in morphological surface and particle size of XFe_2O_4/GO. The images of composite particles indicate the evident agglomeration and close arrangement, with a smooth surface. However, the SEM images show that the $CoFe_2O_4$/GO particles with higher saturation magnetization (4.49 emu/g) are more agglomerated than the $MnFe_2O_4$/GO and $NiFe_2O_4$/GO

particles. These phenomena can be explained by (1) the strong effect of magnetic properties generated from the initial ferrite nanoparticles and (2) the assembly of the primary particles by van der Waals forces [16]. However, the morphologies of XFe_2O_4/GO were still clearly observed with the visual sphere-like shapes, with average particle diameter distributed in the range of approximately 400 to 500 nm. The appearance of blurred white spots covering the nanosheet edge was attributed to the existence of ultrathin graphene layers on the structure [17]. Graphene oxide-doped ferrite can also provide an advantage in terms of adsorption due to its high porosity and the presence of diverse functional groups on the defective surface [18].

Quadratic models for the removal of MB by XFe_2O_4/GO

Second-order polynomial regression equations were established to investigate the influence of the initial concentration, pH, and dosage of XFe_2O_4/GO on the percentage of MB removed. Based on the CCD experimental matrix shown in Table 2, five levels of variables, including the low (encoded − 1), high (encoded + 1) and rotatable (encoded ± α), display the experimental design of 20 runs along

Table 2 Matrix of observed and predicted values for XFe_2O_4/GO (X = Co, Mn, Ni)

Run	Independent factors			Experiment of CR removal (%)			Prediction of MB removal (%)		
	x_1	x_2	x_3	CFG	MFG	NFG	CFG	MFG	NFG
1	80	0.5	5	32.0	24.0	37.0	29.8	25.1	32.9
2	120	0.5	5	24.6	16.6	26.8	22.2	19.0	23.3
3	80	1.5	5	57.5	56.5	79.4	54.4	58.6	76.5
4	120	1.5	5	46.4	40.5	71.5	46.3	41.4	66.9
5	80	0.5	9	33.8	25.6	57.5	32.3	27.7	61.1
6	120	0.5	9	27.4	26.7	47.7	28.9	27.6	49.6
7	80	1.5	9	66.5	52.1	91.3	67.4	52.8	93.8
8	120	1.5	9	62.8	39.6	79.4	63.5	41.5	82.5
9	66.4	1	7	50.8	45.9	84.1	53.6	43.8	84.1
10	133.6	1	7	44.5	31.4	65.0	43.9	29.2	66.4
11	100	0.16	7	14.0	19.7	24.9	16.0	17.3	25.6
12	100	1.84	7	65.5	59.1	89.2	65.7	57.2	89.9
13	100	1	3.6	27.6	36.1	25.9	31.5	33.7	34.4
14	100	1	10.4	49.8	37.9	78.3	48.1	36.0	71.2
15	100	1	7	44.3	28.4	74.7	44.1	27.7	80.3
16	100	1	7	47.9	29.2	77.6	44.1	27.7	80.3
17	100	1	7	45.4	29.1	82.1	44.1	27.7	80.3
18	100	1	7	42.3	24.5	87.3	44.1	27.7	80.3
19	100	1	7	41.5	26.9	79.9	44.1	27.7	80.3
20	100	1	7	43.6	27.6	80.5	44.1	27.7	80.3

CFG, MFG, and NFG are abbreviated for XFe_2O_4/GO (X = Co, Mn, and Ni, respectively)

with the experimental and predicted adsorption results for XFe_2O_4/GO. Thus, empirical relationships between the efficiency of MB removal, the comparison of dye removal efficiency among the different adsorbents, and mathematical interaction of the three independent variables can be described by the following equations:

$$y_{CoFe_2O_4/GO}(\%) = 44.1 - 2.87x_1 + 14.79x_2 + 4.93x_3 - 0.13x_1x_2 + 1.05x_1x_3 + 2.6x_2x_3 + 1.65x_1^2 - 1.15x_2^2 - 1.52x_3^2 \quad (4)$$

$$y_{MnFe_2O_4/GO}(\%) = 27.7 - 4.33x_1 + 11.87x_2 + 0.69x_3 - 2.78x_1x_2 + 1.5x_1x_3 - 2.13x_2x_3 + 3.10x_1^2 + 3.36x_2^2 + 2.52x_3^2 \quad (5)$$

$$y_{NiFe_2O_4/GO}(\%) = 80.3 - 5.27x_1 + 19.09x_2 + 10.93x_3 + 0.03x_1x_2 - 0.45x_1x_3 - 2.7x_2x_3 - 0.79x_1^2 - 7.97x_2^2 - 9.72x_3^2 \quad (6)$$

According to Table 2, the MB removal efficiency varies greatly by nanocomposite material, with the highest mean percentage of dye removal at center points by $NiFe_2O_4$/GO, at nearly 80.3%.

Effect of influential factors on the adsorption of MB onto XFe_2O_4/GO

ANOVA is an essential component in evaluating whether a regression model fits with actual experimental data. Herein, we conducted experimental runs and processed the data using Design-Expert version 9.0.6 (DX9) statistical software to identify the mathematical significance of the main variables. The results of the ANOVA for the quadratic models are listed in Table 3. In general, the proposed models for the three adsorbents were statistically significant at the 95% confidence level, and the response variables were found to be strongly dependent on initial parameters. Specifically, Prob $> F$ or p-values were considerably less than 0.05, while F values for $CoFe_2O_4$/GO, $MnFe_2O_4$/GO, and $NiFe_2O_4$/GO were 48.11, 44.78, and 32.88, respectively. This means that there was only a 0.01% chance of a large F value arising from noise, and hence the models were significant. Moreover, the small F values (1.15, 3.2, and 2.39) of the lack of fit (LOF) values, which were used to measure the failure of a model, confirmed that the quadratic models obtained were significant. Adequate precision ratios, which measure the signal-to-noise ratio, were found to be considerably greater than 4 (25.12, 22.88, and 17.97), indicating an adequate signal and suggesting that these models could be used to navigate the design space. In addition, we examined the data correlation between actual and predicted runs for the materials XFe_2O_4/GO, and these results are shown in Fig. 2. According to this figure, it is evident that data points are well distributed on the straight lines, with coefficients of determination (R^2) and their adjusted values reaching approximately 1.0. This suggests an excellent relationship between experimental and predicted data for all models. Another indication of the adequacy of the model fit is the observation that the plots of residuals against runs were randomly distributed without any patterns or trends (Fig. 3). Hence, these models were ultimately chosen to determine the optimal conditions with respect to the initial concentration, pH, and dosage for achieving the best removal efficiency.

Table 3 ANOVA for response surface quadratic models for XFe_2O_4/GO (X = Co, Mn, Ni)

Response	Source	Sum of squares	Degree of freedom	Mean quare	*F* value	Prob > *F*	Comment
CFG	Model	3595.56	9	399.51	48.11	< 0.0001[a]	SD = 2.88
	x_1	112.49	1	112.49	13.55	0.0042[a]	Mean = 43.41
	x_2	2988.17	1	2988.17	359.85	< 0.0001[a]	CV(%) = 6.64
	x_3	332.00	1	332.00	39.98	< 0.0001[a]	Press = 475.7
	x_1^2	0.13	1	0.13	0.015	0.9048[b]	$R^2 = 0.9774$
	x_2^2	8.82	1	8.82	1.06	0.3270[b]	$R^2_{(adj.)} = 0.9571$
	x_3^2	54.08	1	54.08	6.51	0.0288[a]	$A = 25.21$
	x_1x_2	39.12	1	39.12	4.71	0.0551[b]	
	x_1x_3	18.91	1	18.91	2.28	0.1622[b]	
	x_2x_3	33.16	1	33.16	3.99	0.0736[b]	
	Residuals	83.04	10	8.30	–	–	
	Lack of fit	56.65	5	11.33	2.15	0.2109[b]	
	Pure Error	26.39	5	5.28	–	–	
MFG	Model	2630.98	9	292.33	44.78	< 0.0001[a]	SD = 2.56
	x_1	256.50	1	256.50	39.29	< 0.0001[a]	Mean = 33.87
	x_2	1923.16	1	1923.16	294.60	< 0.0001[a]	CV (%) = 7.54
	x_3	6.51	1	6.51	1.00	0.3416[b]	Press = 402.8
	x_1^2	61.60	1	61.60	9.44	0.0118[a]	$R^2 = 0.9758$
	x_2^2	18.00	1	18.00	2.76	0.1278[b]	$R^2_{(adj.)} = 0.9540$
	x_3^2	36.13	1	36.13	5.53	0.0405[a]	AP = 22.88
	x_1x_2	138.38	1	138.38	21.20	0.0010[a]	
	x_1x_3	163.08	1	163.08	24.98	0.0005[a]	
	x_2x_3	91.18	1	91.18	13.97	0.0039[a]	
	Residuals	65.28	10	6.53	–	–	
	Lack of fit	49.73	5	9.95	3.20	0.1139[b]	
	Pure error	15.55	5	3.11	–	–	
NFG	Model	9127.56	9	1014.17	32.88	< 0.0001[a]	SD = 5.55
	x_1	378.77	1	378.77	12.28	0.0057[a]	Mean = 67.01
	x_2	4978.08	1	4978.08	161.39	< 0.0001[a]	CV(%) = 8.29
	x_3	1632.75	1	1632.75	52.93	< 0.0001[a]	Press = 1786
	x_1^2	0.005	1	0.005	0.00016	0.9901[b]	$R^2 = 0.9673$
	x_2^2	1.62	1	1.62	0.053	0.8234[b]	$R^2_{(adj.)} = 0.9379$
	x_3^2	58.32	1	58.32	1.89	0.1991[b]	AP = 17.97
	x_1x_2	46.00	1	46.00	1.49	0.2500[b]	
	x_1x_3	916.28	1	916.28	29.71	0.0003[a]	

Table 3 continued

Response	Source	Sum of squares	Degree of freedom	Mean quare	F value	Prob > F	Comment
	x_2x_3	1362.63	1	1362.63	44.18	< 0.0001[a]	
	Residuals	308.45	10	30.85	–	–	
	Lack of fit	217.38	5	43.48	2.39	0.1808[b]	
	Pure error	91.07	5	18.21	–	–	

[a]Significant at $p < 0.05$

[b] Insignificant at $p > 0.05$. x_1, x_2, and x_3 are the main factors. x_1^2, x_2^2, and x_3^2 are the square factors. x_1x_2, x_1x_3, and x_2x_3 are the interaction factors

To show the effect of interactive variables on the removal of methylene blue dye using XFe_2O_4/GO as an adsorbent, three-dimensional surface responses were plotted for three input factors, where two factors were allowed to fluctuate in the CCD-based range of given values, and the other factor was maintained at the central level as shown in Figs. 4, 5, and 6. According to Fig. 4a, the elimination of MB displayed an insignificant dependence on the dosage of $MnFe_2O_4$/GO (0.16–1.84 g/L). When the amount of solid increased in the range between 0.16 and 1.84, there was a considerable change in MB removal, with the highest value of 75% obtained at a concentration of 66.4 mg/L and a dosage of 1.84 g/L. Meanwhile, the effect of the interaction of concentration and pH of the solution on MB removal was slightly significant, as shown in Fig. 4b. Regression curves revealed a profound influence of both pH and the dosage of $CoFe_2O_4$/GO on the removal of dye, shown in Fig. 4c. At any constant pH, the addition of adsorbent improved dye uptake, and the removal value increased from 14.5% to roughly 80% at the optimal pH = 10. On the other hand, the effect of pH in solution was largely negligible at a low adsorbent dosage, but increasing both the dosage and pH increased the removal of dye to approximately 76% at a pH of 10.4 and a dosage of 1.84. The increased adsorption of MB upon increasing the pH can be explained by the pHpzc. When pH is lower than pHpzc = 6.4, the positive charge concentrates on the surface of $CoFe_2O_4$/GO, suggesting that electrostatic repulsion emerges between the dye molecule and adsorbent, and hence the removal efficiency of dye adsorption decreases. In contrast, if the pH of the solution is greater than pHpzc, the charge on the surface of the material can transform from positive to negative. This transition may lead to the formation of a complex between cationic compounds, thus enhancing the removal of dye [19].

Figure 5a displays the effect of dosage of $MnFe_2O_4$/GO (0.16–1.84 g/L) and concentration (66.4–133.6 mg/L) on the removal of MB. Here, dye removal increased toward the low range of concentration and high range of dosage. The dosage of $MnFe_2O_4$/GO played a crucial role in the uptake of dye molecules by the pores or surface of the adsorbent. Increasing the dosage of adsorbent component led to an increase in the number of adsorption sites available, and the availability of more $MnFe_2O_4$/GO active sites resulted in the capture of more dye molecules. On the other hand, the effect of pH and concentration was mostly negligible, and the

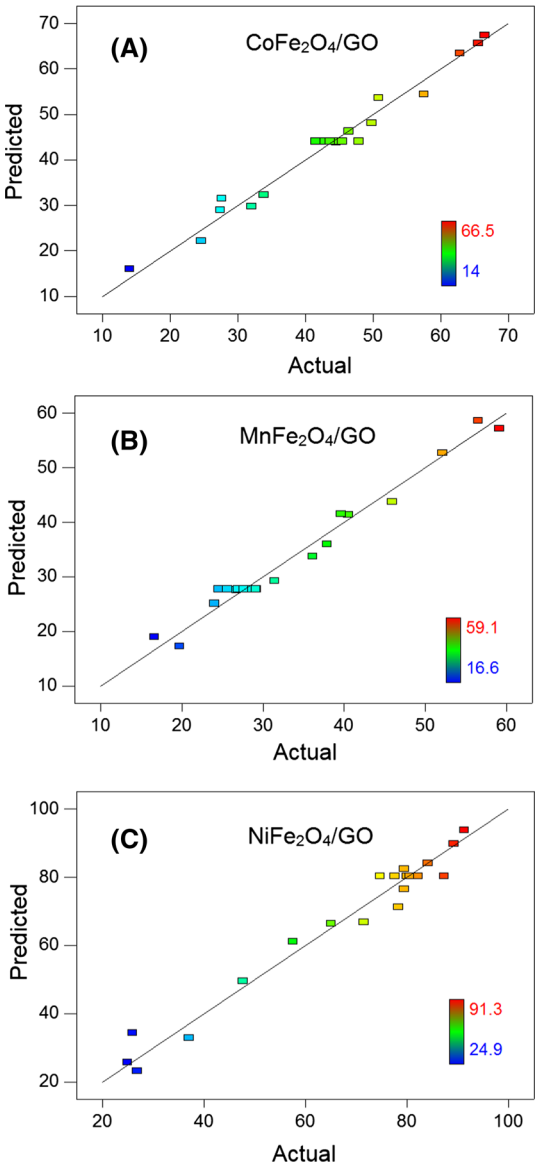

Fig. 2 Actual versus predicted plots (**a**–**c**) for XFe_2O_4/GO (X = Co, Mn, Ni)

reaction only removed a tiny amount of dye from solution, as shown in Fig. 5b. However, there was a marked improvement in the efficiency of dye treatment with increasing dosage of $MnFe_2O_4$/GO, whereas the effect of pH was found to be slightly significant (Fig. 5c). Through the use of 1.84 g/L $MnFe_2O_4$/GO, the predicted removal percentage obtained was 68% at pH = 3.6, which was slightly higher than the batch run conducted at pH = 10.4. For $NiFe_2O_4$/GO, the effect of the three variables was also investigated via RSM. According to Fig. 6, the percentage of MB removal was significantly influenced by the variables. Relative to

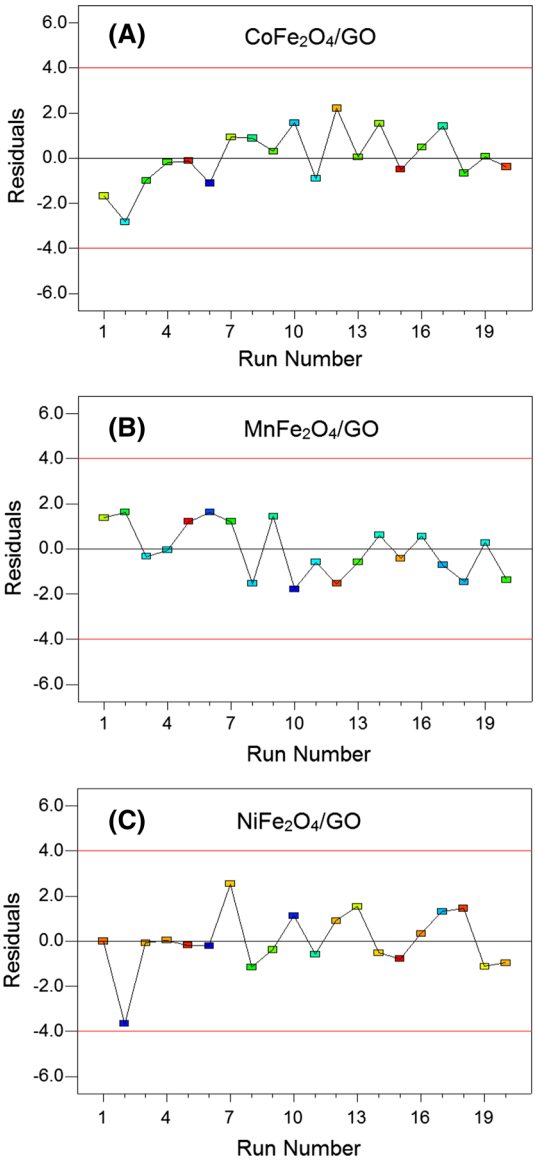

Fig. 3 Residuals versus runs models (**a**–**c**) for XFe_2O_4/GO (X = Co, Mn, Ni)

the other nanomaterials, $NiFe_2O_4$/GO exhibits excellent removal properties when the pH and dosage is increased in conjunction with a decrease in the initial concentration. As a result, removal greater than 90% can be achieved if the adsorption batch conditions allow for a dosage of 1.8 g/L, a pH of 10, and a concentration of 66.4 mg/L. According to the above analysis, the optimal conditions were chosen to maximize the percentage of removal efficiency as presented in Table 4. Repeated experiments experiments were also performed at proposed optimal conditions to verify the accuracy and compatibility of models. As a result,

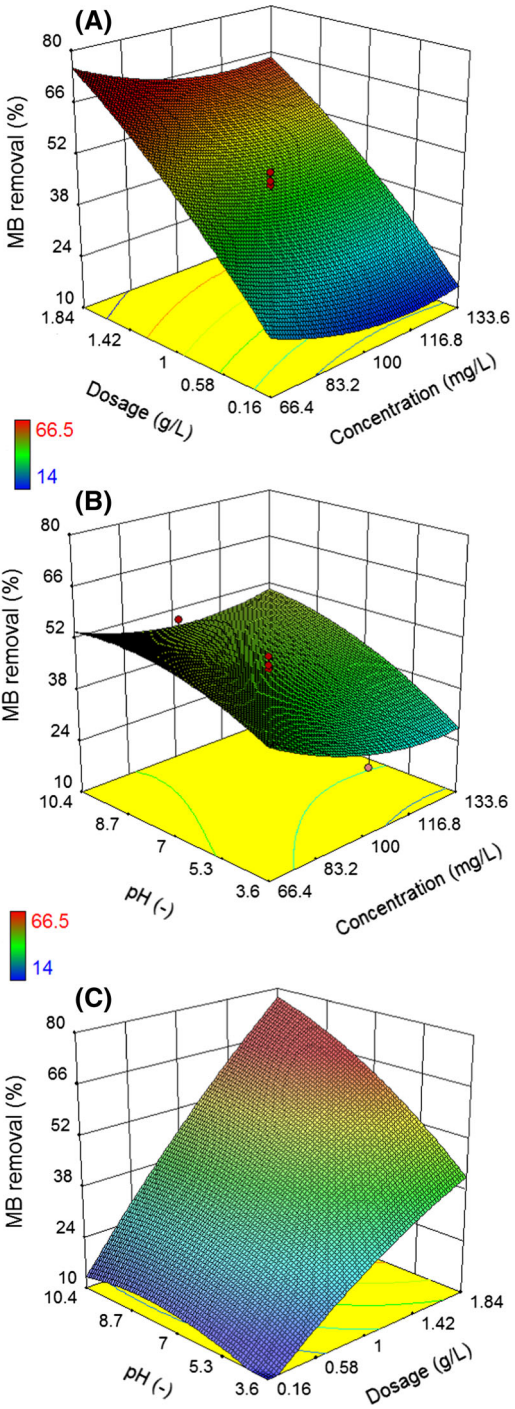

Fig. 4 Surface response plots (**a**–**c**) of the removal of MB by $CoFe_2O_4$/GO

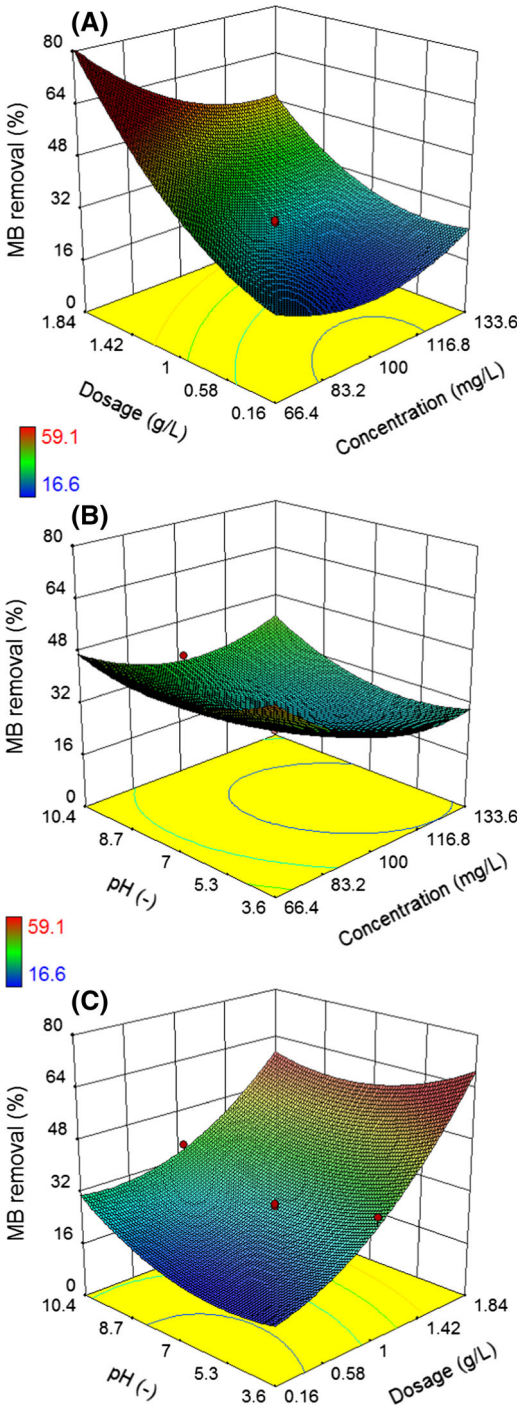

Fig. 5 Surface response plots (**a**–**c**) of the removal of MB by $MnFe_2O_4$/GO

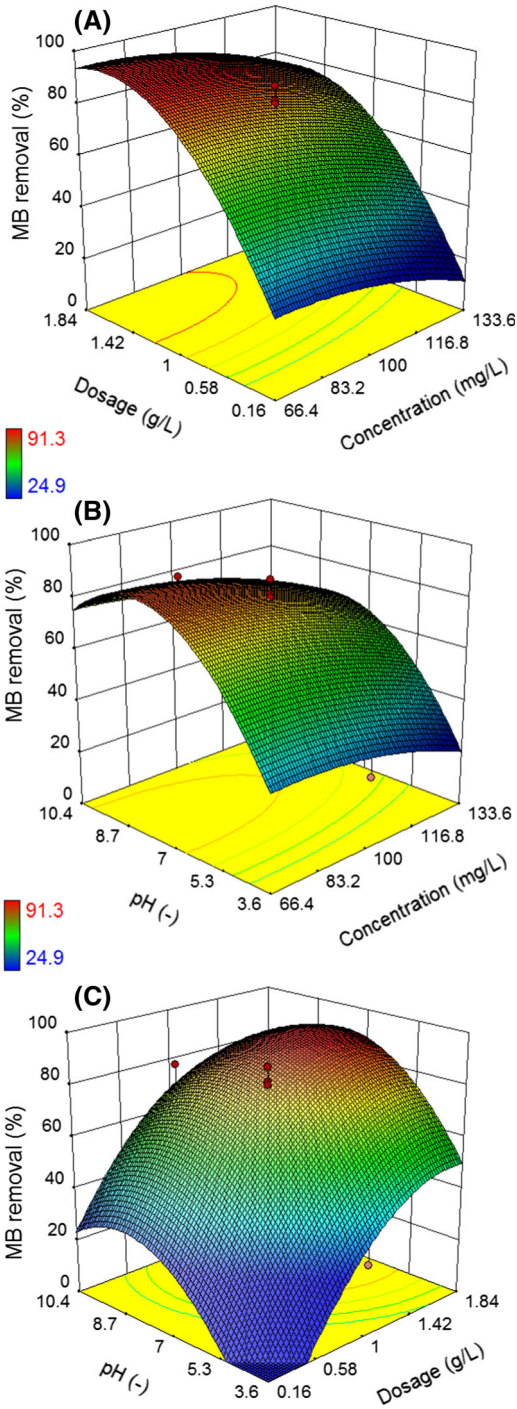

Fig. 6 Surface response plot of the removal of MB by $NiFe_2O_4$/GO

Table 4 Model confirmation

Sample	Concentration (ppm)	Dosage (g/L)	pH	Removal (%)			Desirability
				Predicted	Tested	Error (%)	
CFO/GO	132.5	1.80	10.1	77.3	80.3	3.9	1.0
MFO/GO	89.5	1.79	9.9	60.5	60.1	0.7	1.0
NFO/GO	91.0	1.22	7.9	91.8	87.7	4.5	1.0

the tested maximum removal obeys the following order: 60.1% (X = Mn) < 80.3% (X = Ni) < 91.8% (X = Ni) for the XFe_2O_4/GO adsorbents. Again, these experimental results are in good agreement with the predicted values, thus indicating the very high suitability of the suggested models (Fig. 7).

Adsorption kinetics and effect of contact time

Effect of contact time

Based on the optimization table, we conducted the actual experiments to investigate the effect of contact time and find the equilibrium time for adsorption (Fig. 8). The adsorption of MB onto nanocomposites at various times is displayed in Fig. 8a. After the first 60 min, the MB dye was decolored rapidly; however, the adsorption rate then decreased significantly, and an equilibrium was established after 180 min for all XFe_2O_4/GO adsorbents. In addition, the uptake capacity of $NiFe_2O_4$/GO was slightly higher than that for $CoFe_2O_4$/GO, while the amount of dye adsorbed by $MnFe_2O_4$/GO was significantly lower under the optimal conditions. Thus, the equilibrium capacity of XFe_2O_4/GO for MB followed the trend: $MnFe_2O_4$/GO (29.4 mg/g) < $CoFe_2O_4$/GO (59.8 mg/g) < $NiFe_2O_4$/GO (63.7 mg/g).

Adsorption kinetics

The adsorption rate is considered an important factor related to the heterogeneous phase and physicochemical characteristics of solids in kinetic studies, which describe the mechanism of adsorption processes via kinetic equations. The pseudo-first-order model (Eq. 7), pseudo-second-order model (Eq. 8), the Elovich model (Eq. 10), Bangham's equations (Eq. 11), and the Weber–Morris model (Eq. 12) were used to investigate experimental data, and their respective constants are shown in Fig. 8b–f and Table 5.

$$\log\left(q_e - q_t\right) = \log\, q_e - \frac{k_1 \cdot t}{2.303}, \tag{7}$$

where q_t (mg/g) is the amount of adsorbate adsorbed at the time t (min), q_e (mg/g) is the adsorption capacity at the equilibrium time, and k_1 (min^{-1}) is the pseudo-first-order rate constant.

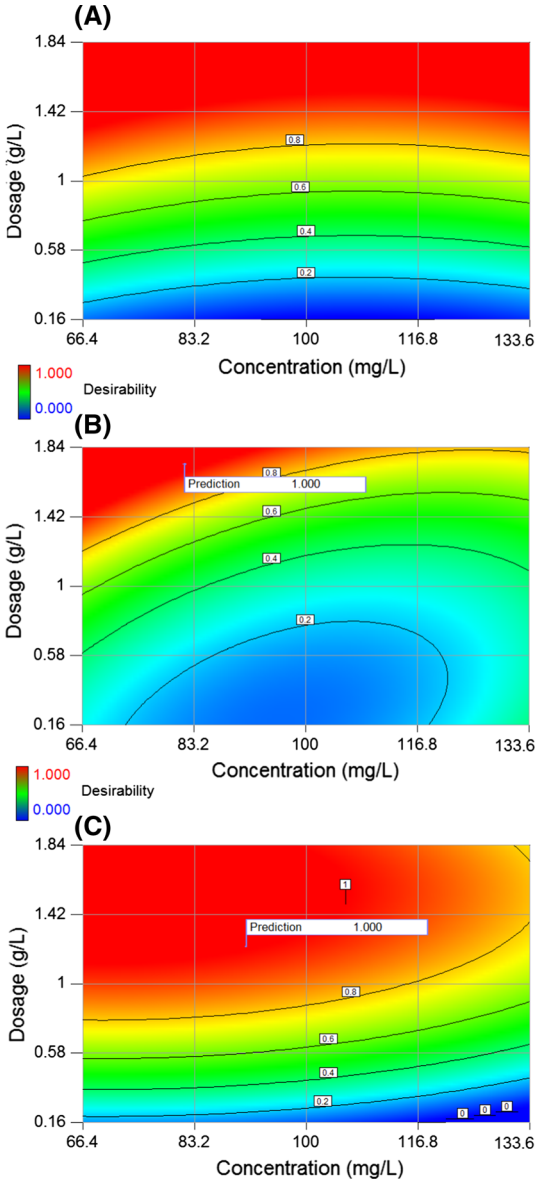

Fig. 7 Desirability for the optimization of the MB removal by XFe_2O_4/GO (X = Co, Mn, Ni)

$$\frac{t}{q_t} = \frac{1}{k_2 \cdot q_e^2} + \frac{t}{q_e} \tag{8}$$

where k_2 (g/mg min) is the pseudo-second-order rate constant, and the initial adsorption rate H:

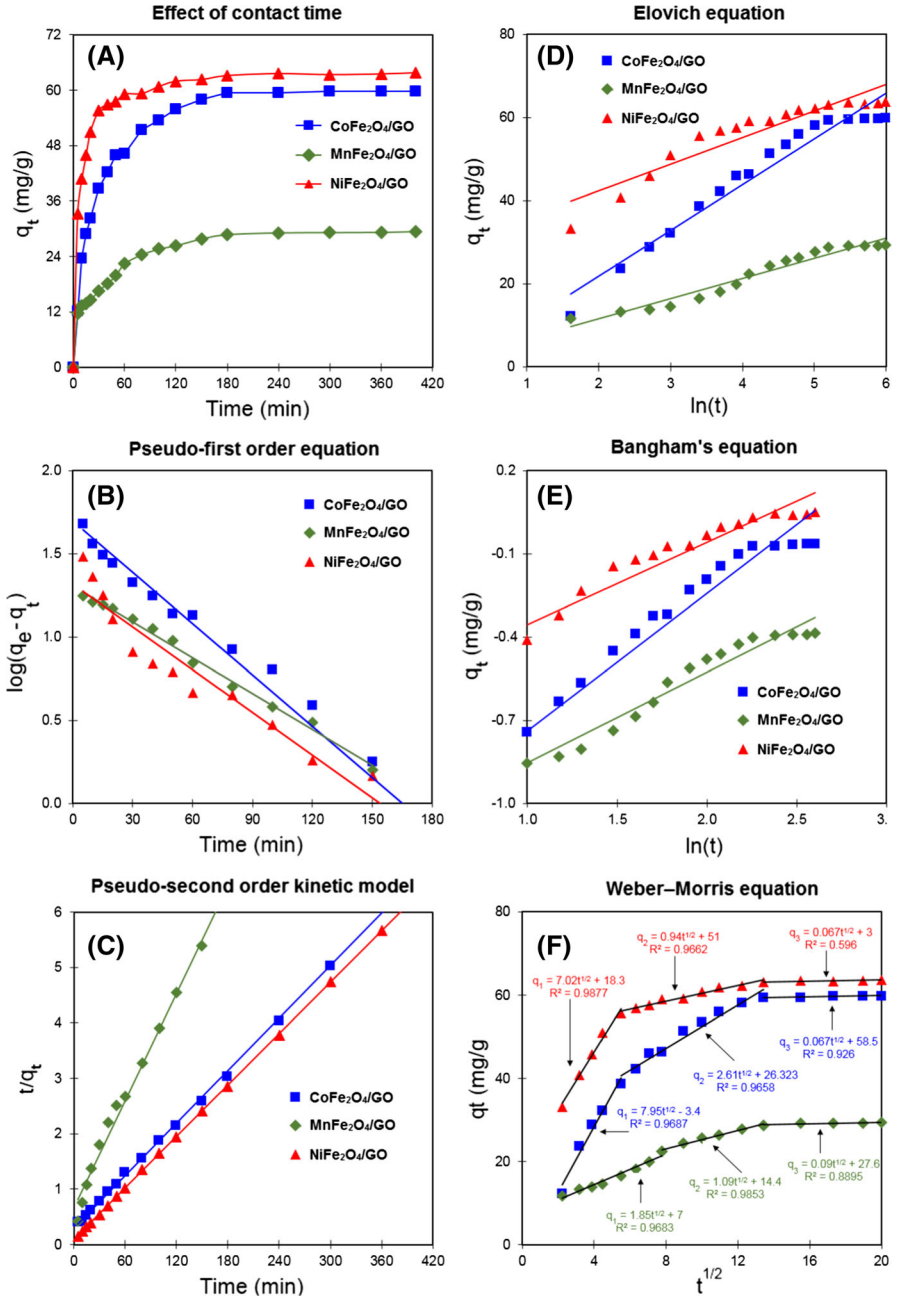

Fig. 8 Effect of time (**a**) and adsorption kinetic models (**b–f**) for XFe_2O_4/GO (X = Co, Mn, Ni) with experimental conditions C_o, dosage, and pH based on the optimization Table 4

Table 5 Kinetics constants for the adsorption of XFe_2O_4/GO (X = Co, Mn, Ni)

Kinetic models	Parameters	Unit	$CoFe_2O_4$/GO	$MnFe_2O_4$/GO	$NiFe_2O_4$/GO
Pseudo-first-order model	k_1	1/min	0.024	0.017	0.019
	q_e	mg/g	49.450	20.140	20.600
	R^2	–	0.970	0.994	0.947
Pseudo-second-order model	k_2	10^4 mg/g min	8.760	15.890	27.810
	q_e	mg/g	63.290	31.060	64.520
	$H = k_2 q_e^2$	–	3.510	1.530	11.570
	R^2	–	0.999	0.998	1.000
Elovich model	β	g/mg	11.009	4.880	6.390
	α	mg/g min	0.089	0.296	15.995
	R^2	–	0.953	0.954	0.871
Bangham's equation	k_B	–	3.740	4.250	21.010
	α_B	–	0.496	0.326	0.297
	R^2	–	0.934	0.958	0.919
Weber–Morris equation	k_1	mg/g min	7.946	1.850	7.024
	R_1^2	–	0.969	0.968	0.988
	k_2	mg/g min	2.61	1.086	0.938
	R_2^2	–	0.966	0.985	0.9662
	k_3	mg/g min	0.067	0.088	0.067
	R_3^2	–	0.596	0.889	0.596

$$H = k_2 \cdot q_e^2 \tag{9}$$

$$q_t = \beta \cdot \ln(\alpha \cdot \beta) + \beta \cdot \ln(t) \tag{10}$$

where α (mg/g min) is the initial adsorption rate, and β (g/mg) is the desorption constant.

$$\log\log\left(\frac{C_o}{C_o - q_t \cdot m}\right) = \log\left(\frac{k_B}{2.303 \cdot V}\right) + \alpha_B \cdot \log(t) \tag{11}$$

where C_o (mg/L) is the initial concentration of MB in solution, V (mL) is the volume of solution, m (g/L) is the dosage of XFe_2O_4/GO, and α_B and k_B are constants of Bangham's equation which can be obtained from the slope and intercept, respectively.

$$q_t = k \cdot t^{1/2} + A \tag{12}$$

where k (mg/g.min) is the intra-particle diffusion rate constant, and A (mg/g) is the constant proportional to the extent of boundary layer thickness [20].

According to Table 5 and Fig. 8b, c, both pseudo-first-order and pseudo-second-order models exhibited a good fit with experimental data when their correlation

coefficients were calculated to be $R^2 > 0.9$. However, pseudo-second-order equations were applied to predict the adsorption kinetics because of their better compatibility R^2 than pseudo-first-order equations for all adsorbents, in addition to the fact that the theoretical q_e in the case of pseudo-second-order equations matched the experimental values better than pseudo-first-order equations: 49.45 versus 63.29 mg/g for $CoFe_2O_4$/GO, 20.14 versus 31.06 mg/g for $MnFe_2O_4$/GO, and 20.6 versus 64.52 mg/g for $NiFe_2O_4$/GO (Table 5). Moreover, the adsorption of MB onto XFe_2O_4/GO was an irreversible process, suggesting that the adsorption rate was controlled by chemisorption via the mechanism of electron exchange between adsorbate and adsorbent by a chemisorption bond [21].

The Elovich equation can be used to explain chemical adsorption processes, in which a solid/gas adsorption system is studied through heterogeneous adsorbing surfaces [22], while Bangham's equation describes the adsorbate pore diffusion behavior [23]. As shown in Table 5 and Fig. 8d, the Elovich equations for the adsorption of dye onto XFe_2O_4/GO exhibited a strong confidence of $R^2 > 0.8$, implying the probability of the chemical adsorption mechanism. The linear curves for Bangham's equation with $R^2 > 0.9$ revealed that the diffusion of XFe_2O_4/GO into pores was not the only rate-controlling step (Fig. 8e) [24].

In the intra-particle diffusion study, the Weber–Morris equation was used to describe the intra-particle diffusion [25]. According to Fig. 8f, regressions of q_t versus $t^{1/2}$ are not linear; hence there are three linearities observed in every curve, indicating that the adsorption of dye onto XFe_2O_4/GO is subject to three steps with different intra-particle diffusion routes. A higher value of k indicates an enhanced rate of adsorption, and the diffusion rates generally decrease against $t^{1/2}$ in the order: $k_1 > k_2 > k_3$. Initially (0–60 min), the rate of diffusion of MB onto XFe_2O_4/GO is high due to the potentially fast surface adsorption at the available active sites of XFe_2O_4/GO. Second and third portions are assigned to the gradual layer adsorption stages, in which the intervention of inter-ionic attraction and molecular association on the thick layer of the surface may increase the electrostatic repulsion and decrease pore volume. Because the intercepts of lines in the first step of the adsorption of MB onto XFe_2O_4/GO do not pass over the origin coordinate, the adsorption rate depends greatly on the intra-particle diffusion, but it is not the only rate-controlling step [26].

Adsorption isotherms

To describe the monolayer adsorption behavior of the nanocomposites, the Langmuir model was employed based on the assumption that the adsorption mechanism occurs on the homogeneous surface with a finite number of adsorption sites. Thus, the Langmuir equation is expressed as follows:

$$\frac{1}{q_e} = \frac{1}{q_m K_L} \cdot \frac{1}{C_e} + \frac{1}{q_m} \tag{13}$$

where C_e (mg/L) and q_e (mg/g) are the equilibrium concentration and adsorption capacity, respectively. The values q_m (mg/g) and K_L (L/mg) are the maximum

adsorption capacity and rate of adsorption (Langmuir constant), respectively. The term of constant separation factor (R_L) is an essential dimensionless equilibrium parameter of the Langmuir isotherm model which is defined by the following equation:

$$R_L = \frac{1}{1 + K_L C_o} \tag{14}$$

where K_L (L/mg) is the Langmuir constant and C_o (mg/L) is the highest initial metal ion concentration. The R_L value-based isotherm is determined as follows: $0 < R_L < 1$ presents a favorable adsorption process; however, a value of $R_L > 1$ is considered to be an unfavorable process. Alternatively, the adsorption isotherm is linear or irreversible if R_L is found to be 1 and 0, respectively.

Multilayer adsorption processes on heterogeneous surfaces were described by the Freundlich model, which assumes the relationship between non-ideal and reversible adsorption occurs at different energies. The empirical equation is as follows:

$$\ln q_e = \ln K_F + \frac{1}{n} \ln C_e \tag{15}$$

where *1/n* and K_F [(mg/g)(L/mg)$^{1/n}$] are Freundlich constants related to the favorability of the adsorption process and the adsorption capacity of the adsorbent, respectively. The slope (value of $1/n$) ranges between 0 and 1 and is a descriptor of adsorption intensity or surface heterogeneity. As the value of the slope approaches zero, the heterogeneity of the process increases, whereas a value below unity implies a chemisorption process. A slope value greater than 1 indicates cooperative adsorption (a physical process).

Temkin modeling is described by the following equation:

$$q_e = B_T \ln K_T + B_T \ln C_e \tag{16}$$

$$B_T = \frac{RT}{b} \tag{17}$$

where K_T (L/g) and b (J/mol) are the Temkin equilibrium constant (L/mol) and the constant B_T related to the heat of adsorption, respectively. R is the gas constant (8.314 J mol^{-1} K^{-1}).

The Dubinin and Radushkevich (D–R) model is widely used to determine the nature of adsorption processes characterized by the adsorption of subcritical vapors onto micro-pores, followed by a pore-filling mechanism:

$$\ln q_e = \ln q_m - B\varepsilon^2 \tag{18}$$

where B (mol^2 kJ^{-2}) is the activity coefficient related to the mean adsorption energy, and q_m (mg/g) is the maximum adsorption capacity. The value ε (kJ^2 mol^2) is the Polanyi potential, which can be calculated from the following equation:

$$\varepsilon = RT \ln\left(1 + \frac{1}{C_e}\right) \tag{19}$$

The apparent energy of adsorption E (kJ mol^{-1}) is the free energy required to transform 1 mole of metal ions from the solution to the surface of the adsorption process:

$$E = \frac{1}{\sqrt{-2B}} \tag{20}$$

Table 6 reports the various constants obtained from the isotherm plots (Fig. 9). Calculated coefficients from models were found to be more than 0.8 for XFe_2O_4/GO for three models. The fitness for adsorption isotherm models was as follows: Langmuir > Freundlich > Temkin > R–D. As a result, the Langmuir model was used to describe the MB adsorption onto XFe_2O_4/GO, and R_L was less than 1.0, indicating that the adsorption process was favorable. This suggests that the adsorption process occurs mainly via monolayer and homogenous adsorption. From the Langmuir equation, the maximum monolayer q_m for uptake of MB onto XFe_2O_4/GO was determined and indicated higher performance than q_m from earlier reports [27–33] (Table 7).

Thermodynamic and leaching test study

The thermodynamic coefficients can be used to describe the adsorption process, and the standard parameters can be represented as follows:

Table 6 Adsorption isotherm constants for XFe_2O_4/GO (X = Co, Mn, Ni)

Kinetic models	Parameters	Unit	$CoFe_2O_4$/GO	$MnFe_2O_4$/GO	$NiFe_2O_4$/GO
Langmuir isotherm	k_L	L/mg	0.020	0.039	0.171
	q_m	mg/g	80.600	42.200	78.100
	R_L	–	0.275	0.224	0.061
	R^2	–	0.960	0.838	0.928
Freundlich isotherm	k_F	mg/g	4.240	6.960	27.560
	$1/n$	–	0.574	0.352	0.256
	R^2	–	0.957	0.826	0.909
Temkin isotherm	k_T	L/mg	0.140	0.350	2.980
	B_T	–	20.670	9.650	14.640
	R^2	–	0.928	0.8164	0.905
Dubinin–Radushkevich (D–R)	B	kJ^2/mol^2	67.650	61.870	5.110
	q_m	mg/g	47.680	32.950	66.870
	E	kJ/mol	0.086	0.090	0.313
	R^2	–	0.901	0.816	0.867

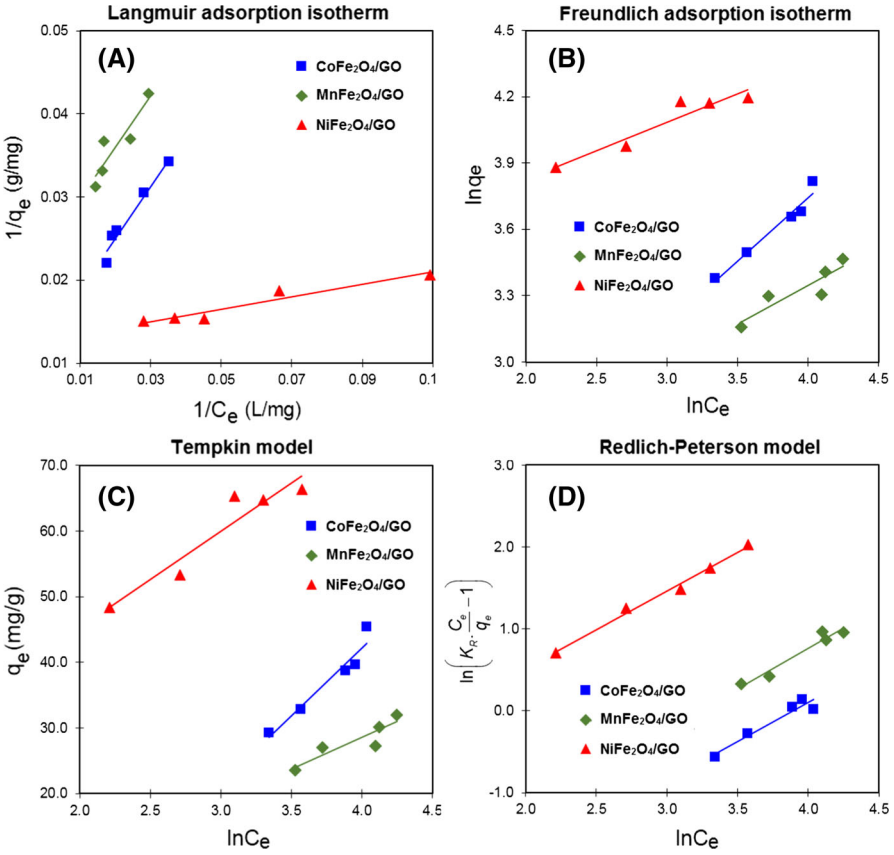

Fig. 9 The curves of adsorption isotherm models (**a**–**d**) for XFe_2O_4/GO (X = Co, Mn, Ni)

$$\Delta G = -RT \ln K_C \tag{21}$$

where K_C is the adsorption equilibrium constant and T (K) is the temperature at the equilibrium point. K_C is the ratio of the equilibrium concentration of adsorbent in the liquid and solid phases and can be determined as follows:

$$\ln K_C = \frac{C_A}{C_e} \tag{22}$$

where C_A and C_e (ppm) are the equilibrium concentrations in aqueous solution of organic dyes adsorbed onto the adsorbent, respectively. The standard enthalpy (ΔH) and entropy (ΔS) can be calculated by the Van 't Hoff isotherm equation as follows:

$$\ln K_C = \left(\frac{-\Delta H}{R}\right) \cdot \frac{1}{T} + \frac{\Delta S}{R} \tag{23}$$

Figure 10a shows a comparison of the thermodynamic model for three materials which describes the effect of a wide range of temperatures (293–323 K) on the

Table 7 A comparison of the characteristics and adsorption capacity of the nanocomposites with those from other studies

No.	Nanocomposites	S_{BET} (m^2/g)	pH	Equilibrium time (min)	q_m (mg/g)	Ref.
1	$CoFe_2O_4$/GO	239.57	10.1	180	80.6	This work
2	$MnFe_2O_4$/GO	246.39	9.9	180	42.2	This work
3	$NiFe_2O_4$/GO	181.12	7.9	180	78.1	This work
4	γ-Fe_2O_3/SiO_2	74.30	7–12	240	23.4	[27]
5	Chitosan/Fe_3O_4/graphene oxide (CS/Fe_3O_4/GO)	–	10.5	40	30.1	[28]
6	Magnetic graphene/calcium alginate (G-Fe_3O_4/CA)	–	6	180	37.04	[29]
7	Poly(3,4-propylenedioxythiophene)/MnO_2 composites	–	–	60	13.94	[30]
8	Graphene nanosheet/magnetite (GNS/Fe_3O_4)	–	11	20	43.82	[31]
9	OMWCNT- Fe_3O_4	169.00	6.5	240	41.50	[32]
10	OMWCNT-κ-carrageenan-Fe_3O_4	142.20	6.5	240	46.36	[32]
11	Magnetic multi-wall carbon nanotube (Fe_3O_4-MMWCNT)	61.74	7	360	15.74	[33]

adsorption capacity of XFe_2O_4/GO. From the Van 't Hoff equation with $R^2 > 0.9$, the thermodynamic constants of enthalpy, entropy, and Gibbs free energy variations were determined. According to Table 8, the positive values of ΔH revealing the endothermic state of adsorption and the positive ΔS show the high affinity of MB for

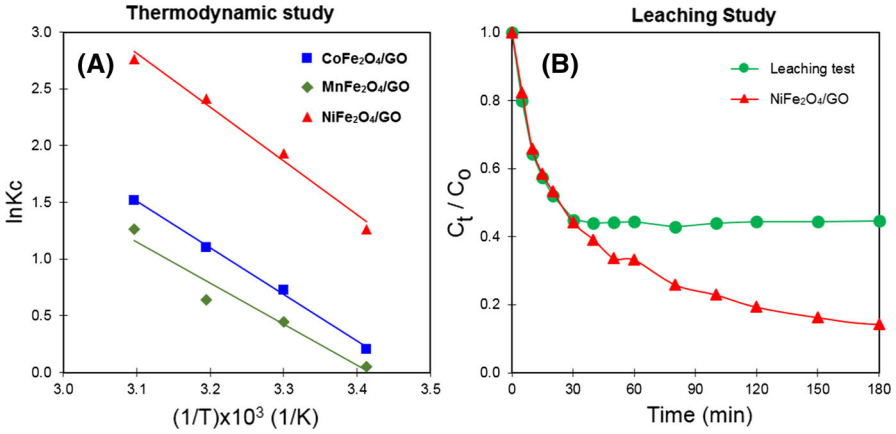

Fig. 10 Curves of the thermodynamic study (**a**) for XFe_2O_4/GO (X = Co, Mn, Ni) and (**b**) leaching test study for $NiFe_2O_4$/GO

XFe_2O_4/GO, while the negative value of ΔG at the investigated temperatures implies that the adsorption can occur readily at these temperatures.

The leaching test is an important experiment for confirming the heterogeneity of adsorbents or catalysts in the reaction media. This test was conducted as follows: The $NiFe_2O_4$/GO nanocomposite (0.05 mg) was first poured into an Erlenmeyer flask containing 50 mL MB dye (100 mg/L). After stirring for 30 min, the solid was separated completely by magnetic and centrifugal (3000/min rate for 10 min) methods. Afterwards, the residual solution was stirred for 120 min, and the dye concentration was monitored using UV–Vis spectroscopy at different intervals. A plot of C_t/C_o against t (min) was recorded and is shown in Fig. 10b. At 30 min, the leaching test curve shows that the C_t/C_o ratio was approximately 0.4. However, no further change in the C_t/C_o ratio was observed after the $NiFe_2O_4$/GO nanocomposite was removed from the solution. Therefore, it is likely that the adsorption process can only occur in the presence of the solid $NiFe_2O_4$/GO, and the leaching of GO, $NiFe_2O_4$, or $NiFe_2O_4$/GO into the aqueous phase should not contribute to the process.

Desorption and regeneration studies

Desorption of MB from MB-loaded $NiFe_2O_4$/GO was conducted using different organic and inorganic eluents including ethanol, acetone, H_2O, KOH 0.1 M, and HCl 0.1 M, with the goal of finding an efficient and inexpensive solvent suitable for the regeneration of materials. Here, 10 mL of eluents was added to a beaker containing 0.05 g of MB-loaded $NiFe_2O_4$/GO. The mixtures were then stirred for 10 min, and the nanocomposites were magnetically removed from the solution. Afterwards, dye concentration was checked using UV–Vis spectroscopy. The results show that ethanol is a potential solvent for the removal of the MB dye, with desorption efficiency of 97%. Importantly, this regeneration study demonstrates that the novel material described herein can be recycled practically. Thus, XFe_2O_4/GO was reused several times using absolute ethanol as a desorption solvent. Figure 11 shows the results from five cycles of experiments conducted in the batch mode. The percentage of MB dye removal decreased from 80.5 to 54.8%, 60.1 to 34.2%, and 87.7 to 40.5% for XFe_2O_4/GO (X = Co, Mn, and Ni, respectively).

Table 8 Thermodynamic parameters for the adsorption of XFe_2O_4/GO (X = Co, Mn, Ni)

Parameters	Unit	$CoFe_2O_4$/GO	$MnFe_2O_4$/GO	$NiFe_2O_4$/GO
ΔH	J/mol	34076.60	29973.60	39789.300
ΔS	J/mol K	118.17	102.450	145.25
ΔG_{293}	J/mol	− 546.30	− 42.80	− 2767.7
ΔG_{303}	J/mol	− 1728.00	− 1067.20	− 4220.10
ΔG_{313}	J/mol	− 2909.60	− 2091.70	− 5672.60
ΔG_{323}	J/mol	− 4091.30	− 3116.10	− 7125.00
R^2	–	0.9975	0.9498	0.9868

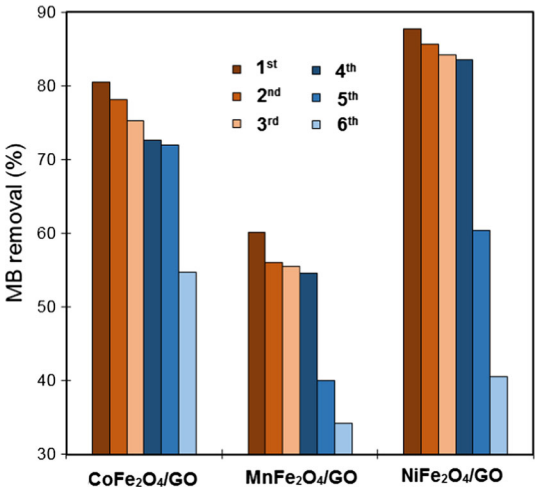

Fig. 11 Recyclability experiment for XFe_2O_4/GO (X = Co, Mn, Ni)

Conclusion

The present study demonstrated improved removal efficiency for MB through the application of a mathematical tool for optimizing the adsorption of nanocomposites composed of ferrite with different metal sites XFe_2O_4 (X = Co, Mn, Ni) and GO. Under the optimal conditions achieved, the order of dye removal efficiency was as follows: 60.1% ($MnFe_2O_4$/GO) < 80.3% ($CoFe_2O_4$/GO) < 91.8% ($NiFe_2O_4$/GO). The kinetics of the adsorption process were shown to fit well with pseudo-second-order models for all materials, and hence adsorption is assumed to be a chemisorption process. The isotherm data examined show that the adsorption behavior is mainly monolayer and displays a good correlation with Langmuir models. The adsorbents could be regenerated and reused for at least four cycles, which underscores the potential utility of nanocomposites containing Co, Mn, and Ni metal sites as materials for dye treatment.

Acknowledgements This work was supported by the Foundation for Science and Technology Development funded by the Ministry of Education and Training (grant no. 01/HD-B-2016-NTT).

References

1. V.K. Gupta, Suhas, J. Environ. Manag. **90**, 2313 (2009)
2. B. Song, G. Zeng, J. Gong, J. Liang, P. Xu, Z. Liu, Y. Zhang, C. Zhang, M. Cheng, Y. Liu, S. Ye, H. Yi, X. Ren, Environ. Int. **105**, 43 (2017)
3. F. Perreault, A.F. De Faria, S. Nejati, M. Elimelech, ACS Nano **9**, 7226 (2015)
4. V.T. Tran, T.P.Q. Bui, D.T. Nguyen, T.H.N. Le, L.G. Bach, Water Sci. Technol. **75**, 2047 (2017)
5. V.T. Tran, T.P.Q. Bui, D.T. Nguyen, T.T.V. Ho, L.G. Bach, Surf. Interfaces **6**, 209 (2017)
6. N.I. Zaaba, K.L. Foo, U. Hashim, S.J. Tan, W. Liu, C.H. Voon, Procedia Eng. **184**, 469 (2017)
7. P.C.R. Varma, R.S. Manna, D. Banerjee, M.R. Varma, K.G. Suresh, A.K. Nigam, J. Alloys Compd. **453**, 298 (2008)
8. C. Tan, X. Huang, H. Zhang, Mater. Today **16**, 29 (2013)
9. V.T. Tran, T.P.Q. Bui, D.T. Nguyen, T.H.N. Le, L.G. Bach, Adsorpt. Sci. Technol. **35**, 72 (2017)

10. Y. Yao, S. Miao, S. Liu, L. Ping, H. Sun, S. Wang, Chem. Eng. J. **184**, 326 (2012)
11. K. Vasundhara, S.N. Achary, S.K. Deshpande, P.D. Babu, S.S. Meena, K. Vasundhara, S.N. Achary, S.K. Deshpande, P.D. Babu, S.S. Meena, J. Appl. Phys. **113**, 194101 (2013)
12. P. Kollu, P.R. Kumar, C. Santosh, D.K. Kim, A.N. Grace, RSC Adv. **5**, 63304 (2015)
13. K. Hareesh, B. Shateesh, R.P. Joshi, S.S. Dahiwale, V.N. Bhoraskar, S.K. Haram, S.D. Dhole, Electrochim. Acta **201**, 106 (2016)
14. S.C.-G.S. Yáñez-Vilara, M. Sánchez-Andújara, C. Gómez-Aguirrea, J. Mirab, M.A. Señarís-Rodríguezа, J. Solid State Chem. **182**, 2685 (2009)
15. W. Yin, S. Hao, H. Cao, RSC Adv. **7**, 4062 (2017)
16. W.P. Wang, H. Yang, T. Xian, J.L. Jiang, Mater. Trans. **53**, 1586 (2012)
17. Q. Zhao, H. Zhao, L. Yan, M. Bi, Y. Li, Y. Zhou, Z. Song, T. Jiang, J. Nanosci. Nanotechnol. **17**, 28 (2017)
18. C. Eid, E. Assaf, R. Habchi, P. Miele, M. Bechelany, RSC Adv. **5**, 97849 (2015)
19. M. Khosravi, S. Arabi, Water Sci. Technol. **74**, 343 (2016)
20. Y. Huang, S. Li, J. Chen, X. Zhang, Y. Chen, Appl. Surf. Sci. **293**, 160 (2014)
21. N.V. Sych, S.I. Trofymenko, O.I. Poddubnaya, M.M. Tsyba, V.I. Sapsay, D.O. Klymchuk, A.M. Puziy, Appl. Surf. Sci. **261**, 75 (2012)
22. F. Wu, R. Tseng, R. Juang, Chem. Eng. J. **150**, 366 (2009)
23. A.A. Inyinbor, F.A. Adekola, G.A. Olatunji, Water Resour. Ind. **15**, 14 (2016)
24. G.A.Gh. Ghanizadeh, React. Kinet. Mech. Catal. **102**, 127 (2011)
25. A. Mittal, A. Malviya, D. Kaur, J. Mittal, L. Kurup, J. Hazard. Mater. **148**, 229 (2007)
26. S. Han, K. Liu, L. Hu, F. Teng, P. Yu, Y. Zhu, Sci. Rep. **7**, 43599 (2017)
27. D. Chen, Z. Zeng, Y. Zeng, F. Zhang, M. Wang, Water Resour. Ind. **15**, 1 (2016)
28. H.V. Tran, L.T. Bui, T.T. Dinh, D.H. Le, C.D. Huynh, A.X. Trinh, Mater. Res. Express **4**, 35701 (2017)
29. N. Song, X. Wu, S. Zhong, H. Lin, J. Chen, J. Mol. Liq. **212**, 63 (2015)
30. R. Jamal, L. Zhang, M. Wang, Q. Zhao, T. Abdiryim, Prog. Nat. Sci. Mater. Int. **26**, 32 (2016)
31. L. Ai, C. Zhang, Z. Chen, J. Hazard. Mater. **192**, 1515 (2011)
32. O. Duman, S. Tunc, T.G. Polat, B.K. Bozo, Carbohydr. Polym. **147**, 79 (2016)
33. J. Gong, B. Wang, G. Zeng, C. Yang, C. Niu, Q. Niu, J. Hazard. Mater. **164**(164), 1517 (2009)